16th World Congress in Computational Mechanics (WCCM)
21-26 July 2024, Vancouver, Canada
A. Korobenko, M. Laforet, S. Prudhomme, R. Vaziri (Eds)

A STUDY ON THE STRUCTURAL SYSTEMS WITH TAPERED HARDENING-TYPE HYSTERESIS DEVICES

AGURI NODA[1,2], TOSHIO MAEGAWA[1], SOMA MITSUI[2],

AND MASAMICHI SASATANI[2]

[1] KUMAGAI GUMI CO., LTD,
2-1 Tsukudocho, Shinjuku-ku, Tokyo 162-8557, Japan
(aguri.noda, tmaegawa)@ku.kumagaigumi.co.jp and https://www.kumagaigumi.co.jp/

[2] Tokyo Denki University
5 Senju Asahi-cho, Adachi-ku, Tokyo 120-8551, Japan
(21uda02@ms, 24fma57@ms, sasatani@mail).dendai.ac.jp and https://www.dendai.ac.jp/en/

Key words: Hardening-type hysteresis, Displacement control devices, Expereimental study, FEM.

Abstract. *The Japanese seismic design code allows for formation of plastic hinges at beam ends during large earthquakes. However, in cases in which seismic motion exceeds anticipated levels, seismic energy surpassing the structure's absorption capacity may result in partial destruction, ultimately leading to the collapse of the whole building. Unexpected damage to buildings may also occur if they are subjected to long-period ground motions. To prevent such damage, we propose a displacement control device with hardening-type hysteresis. We performed experiments and analysis to verify the performance.*

1 INTRODUCTION

The current seismic design code in Japan presumes that the formation of plastic hinges at beam ends will result in plastic deformation in a structure, resulting in increased seismic energy absorption capacity of the structure and preventing its collapse. However, in cases in which seismic motions exceed anticipated levels, seismic energy surpassing the structure's absorption capacity may result in partial destruction, ultimately causing the whole building to collapse. In addition, the increased plasticity of the building's members when subjected to seismic motion may increase its natural period, making the building more susceptible to long-period ground motions. Countermeasures to such events are important for protecting human life and allowing continued building use. Studies on methods for mitigating such events are currently underway, including methods to prevent the plasticization of members and methods for ways to control building deformation to prevent excessive deformation. E.g., see 1)

This study focuses on developing a hardening-type hysteresis element as a deformation control member that serves as a safeguard against excessive deformation and provides the building with the safety margin needed to protect against seismic motions exceeding anticipated levels.

2 HARDENING DEVICE

Figure 1 shows schematic illustrations of the hardening-type hysteresis element proposed herein as the deformation control member. This element consists of tapered members, up-thrust members, steel rods, and disc springs. In the initial state, the tapered members are sandwiched between the up-thrust members and secured in place by the disc springs and steel rods. When the tapered members are pushed inwards in the direction of the applied force, the up-thrust members are pushed apart. This transfers the force to the steel rods via the disc springs. When the disc springs are flattened against each other, the load borne by the steel rods increases, resulting in two levels of stiffness. This member is designed to be attached to the moment frame of buildings and to reduce the stiffness of the frame during minor earthquakes, while permitting the frame to demonstrate high stiffness when displacement exceeds a certain point during moderate to major earthquakes.

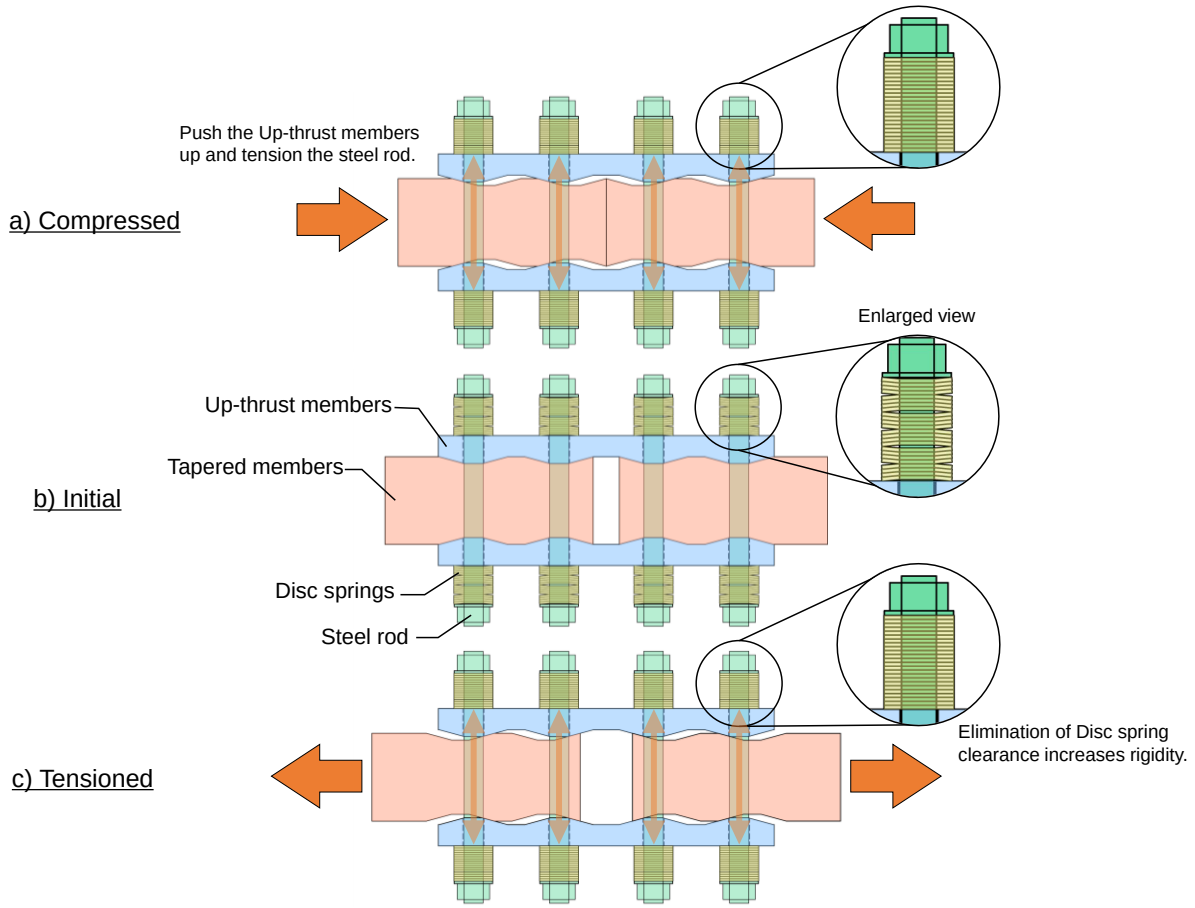

Figure 1: Schematic illustrations of hardening-type hysteresis device

3 PRELIMINARY EXPERIMENT

We undertook an experiment to confirm the basic properties of the proposed hardening mechanism. Presented below are the results of the unidirectional loading experiment on a specimen having a single steel rod.

3.1 Test specimens

Figure 2 shows schematic illustrations of the test specimen and the loading method. The preliminary test specimen consists of a pair of up-thrust members and tapered members serving as the loading jig, which are secured together with disc springs and a steel rod. This setup is adopted to confirm the behavior of the specimen having a single steel rod. Table 1 lists the parameters of the test specimens in this experiment, which include the angle of the tapered member and the condition of the interface between the tapered member and the up-thrust member. The angle of the tapered members was 30° or 60°. We prepared two interface conditions, one milled to realize scale-free conditions and the other with corrosion. The steel rods are made of SNR400B (20 mm dia.) with machined threads. The tapered members and up-thrust members are made of SS400. Made of SUS304-CSP for heavy loads, eight disc springs were placed in a serial configuration. Table 2 gives the mechanical properties of the steel rods. Note that the steel rods were manually tightened. No efforts were made to control tension.

Loading was performed using an Amsler universal testing machine. Photo 1 shows the experimental configuration. The unloading-reloading process was repeated three times within the elastic range of the steel rod. A Teflon® sheet was placed at the contact surface between the up-thrust members and the loading jig to reduce the effects of friction. Absolute displacement was measured at the front and back sides of the tapered member using a displacement gauge. Strain gauges were used to measure the strain on the front and back sides of the steel rods.

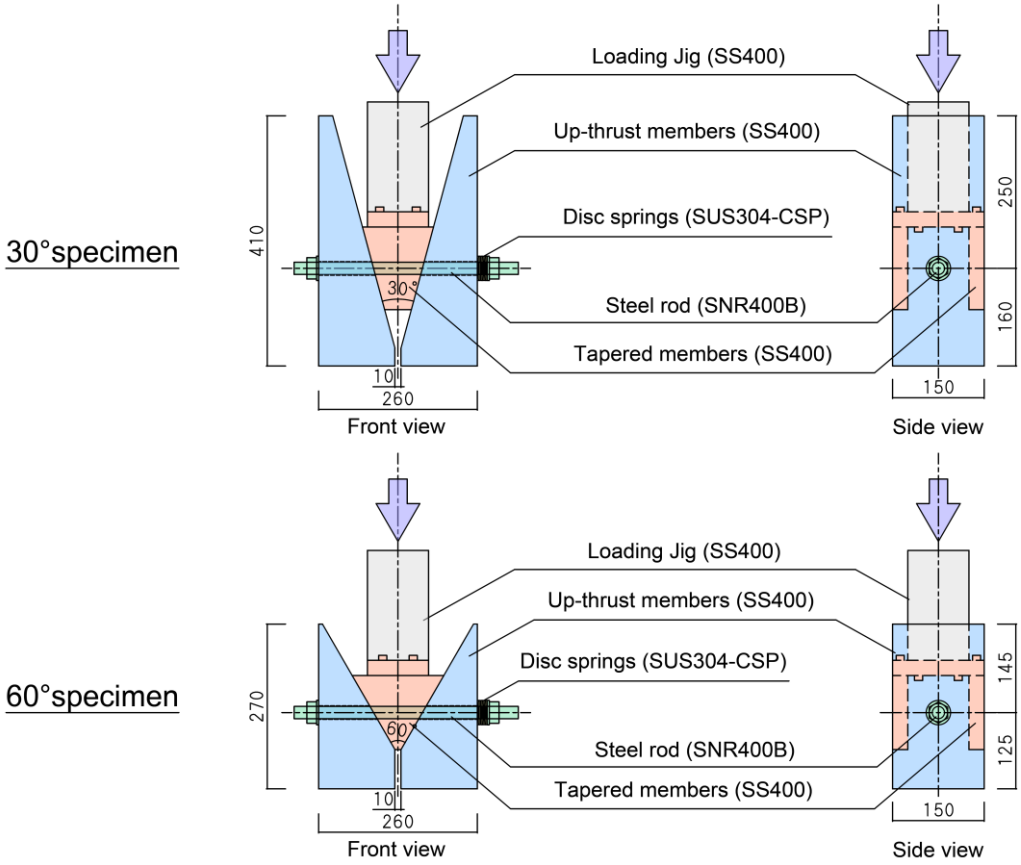

Figure 2: Schematic illustrations of preliminary test specimen

Table 1: Preliminary test parameters

Case	Taper angle	Interface condition	Disc springs	
			Spring constant	Total deflection
60-0 60-1	60°	scale-free rusty	1.04kN/mm	7.2mm
30-0 30-1	30°	scale-free rusty		

Table 2: Mechanical properties of the steel rods

Steel grade	Yield strength N/mm^2	Tensile strength N/mm^2	yield ratio %	Elongation %
SNR400B (φ20)	317	457	69	28

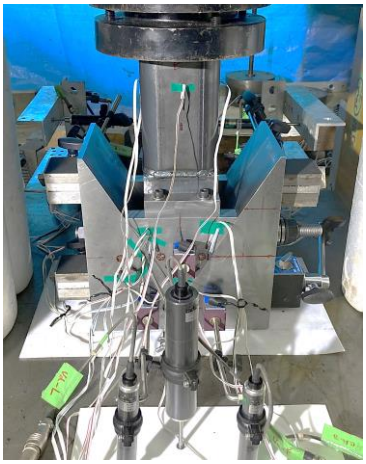

Photo 1: Experimental configuration

3.2 Results and discussions

Figure 3 shows the relationship between vertical load (P) and vertical displacement of the up-thrust members (Vd), the various calculated values, and the relationship between the value of vertical load (T_conv.) obtained by converting the load value (T) calculated based on the strain measured on the steel rod using Equation (1) and the value of vertical displacement (Hd_conv.) obtained by converting the displacement of the expanding up-thrust members (Hd) based on the geometric relationship. The vertical and horizontal axes represent load value and displacement, respectively. We obtained the relationship between vertical load and load value of the steel rods presented in Equation (1) by decomposing the force generated at the tapered section of the tapered member. The calculations assume the coefficient of friction is μ = 0.15 at the interface with the steel members without corrosion treatment and that μ = 0.45 for that with corrosion treatment. The coefficient of friction at the interface between the bottom of the up-thrust members and the specimen support surface is assumed to be μ' = 0.10.

$$P = \frac{2 \times \left(\tan\frac{\theta}{2} + \mu\right)}{1 - \mu \tan\left(\frac{\theta}{2}\right) - 2 \times \mu' \left(\tan\frac{\theta}{2} + \mu\right)} \times T \quad (1)$$

P: Vertical load
θ: Angle of the tapered member
T: Force in the axial direction of the steel rods
μ: Coefficient of friction at the interface with the steel rods
μ': Coefficient of friction at the interface between the bottom of the up-thrust members and the specimen support surface

The vertical displacement at which the disc springs are flattened and in contact with each other is 6.24 mm and 13.44 mm for taper angles of 60° and 30°, respectively. The slope of the stiffness curves in the graphs generally changes near this point, confirming that the slope switches at the predicted position. The experimental values, as well as the first stiffness and second stiffness, are generally consistent with the calculated values. Specimen 30-0 exhibits high P values relative to T_conv. The relationship between T_conv. and Hd_conv. shows that the yield load of the steel rod is generally consistent with the calculated value, indicating that

the load borne by the steel rod is as expected. Thus, the high P values are attributed to greater than expected friction between the wedge and the up-thrust member. The T_conv. obtained for all other specimens indicates the steel rod generally yielded near to the calculated yield load. These results confirm that this device is capable of transferring the vertical load to the steel rods and acquiring secondary stiffness.

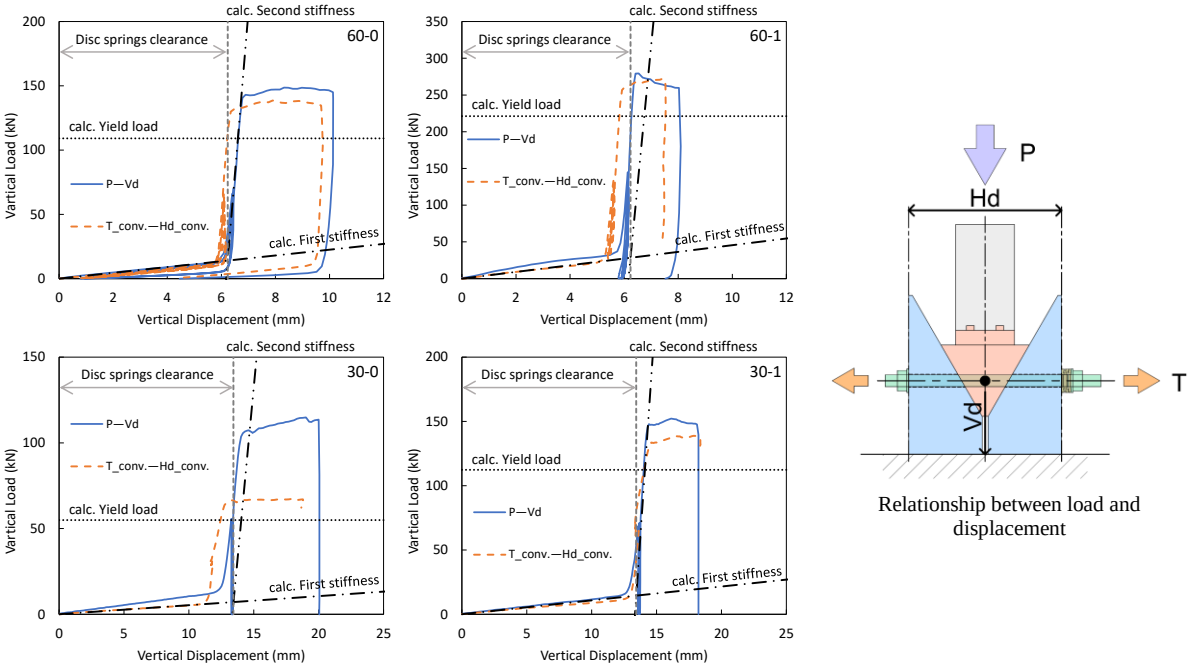

*T is converted into the vertical direction using Equation (1), while Hd is converted into the vertical direction based on geometric relationships.
The converted values are denoted as T_conv. and Hd_conv.

Figure 3: Load to displacement relationship

The effects of the repeated unloading-reloading process on the device differ among the specimens with a taper angle of 60° and depend on the interface condition. For specimen 60-0 with a smooth interface, the displacement responds to unloading and returns to the initial state. However, for specimen 60-1 with a rusty interface, displacement remained unaffected by unloading; the tapered member remained stuck inside the up-thrust member at the end of the test. On the other hand, for specimens with a taper angle of 30°, displacement failed to respond to unloading regardless of the interface condition. This may be because the stiffness of the disc springs is insufficient to retract the up-thrust member. Adjustments of the stiffness of the disc springs may be required to ensure displacement occurs after unloading.

4 ELEMENTAL EXPERIMENT

The preliminary experiment confirmed the basic properties of the hardening device. Thereafter, we proceeded to propose a device design that would allow capacity adjustments by incorporating varying numbers of steel rods when implementing the device within a moment frame. Presented below are the results of a unidirectional loading experiment.

4.1 Test specimens and method of experiment

Figure 4 shows schematic illustrations of the test specimens and the loading method. The elemental specimens consist of multiple steel rods, disc springs, a pair of tapered members, and a pair of up-thrust members. The purpose of this experiment is to investigate the behavior of the device when multiple steel rods are involved. Table 3 lists the specimen parameters. The variables include the angle of the tapered member (30°, 45°, and 60°), the number and combination of disc springs, and the number of steel rods. All interfaces are milled steel surfaces. The steel rods are of SNR400B (φ22 mm). The threads were machined. The tapered members and the up-thrust members are made of SN490B. The disc springs are made of SUS304-CSP for heavy loads. Table 4 presents the mechanical properties of the steel rods. The steel rods were tightened manually. No efforts were made to control tension.

Force was applied via compressional loading using an Amsler-type universal testing machine. As in the preliminary experiment, the unloading-reloading process was repeated three times within the elastic range of the steel rod. Photo 2 shows the experimental setup. We measured the relative displacement between the tapered members using a displacement meter, and the strain on the front and back side of the steel rods using a strain gauge.

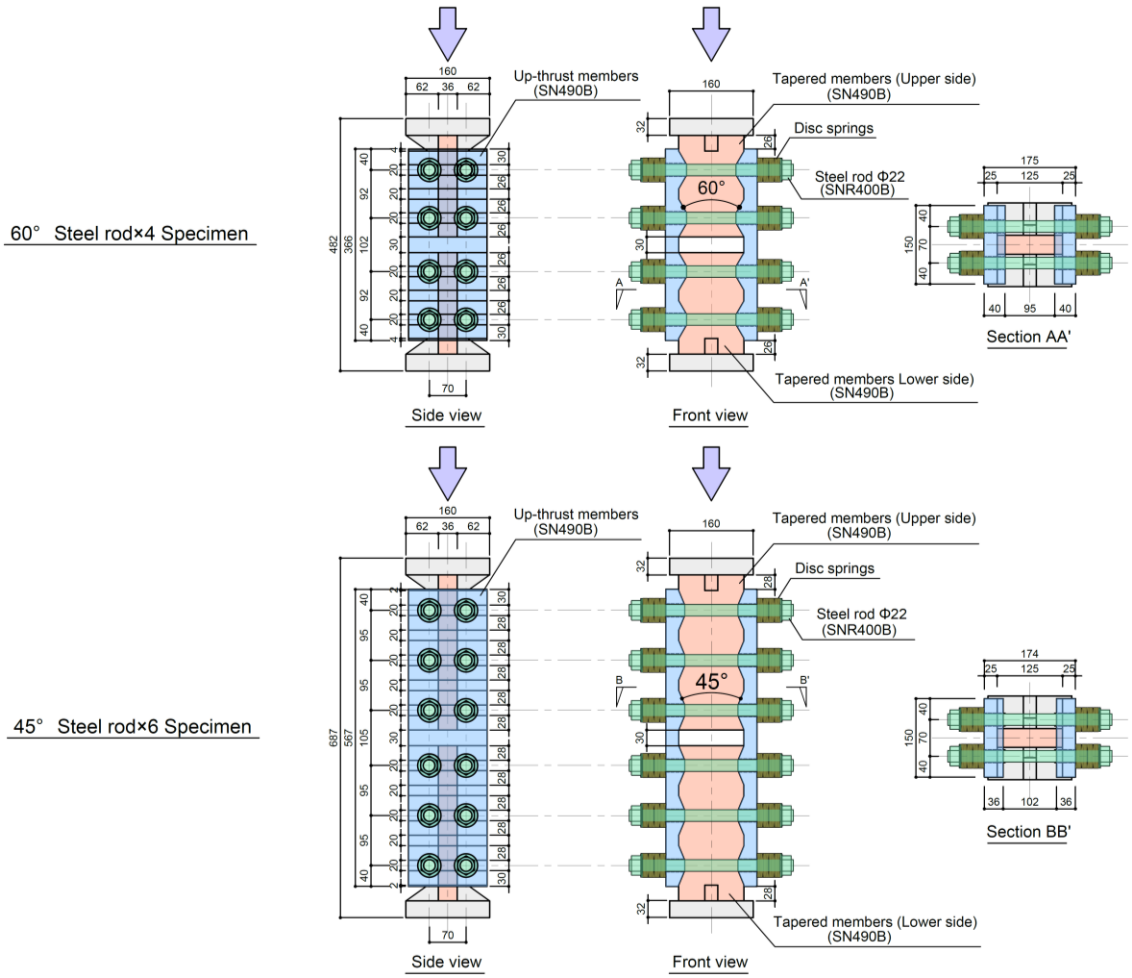

Figure 4: Schematic illustrations of the test specimen

Table 3: Parameters of the elemental specimens

Case	Number of steel bars (Tapered member per piece)	Taper angle °	Disc springs	
			Spring constant kN/mm	Total deflection mm
30-4	4	30	4.81	4
45-4		45		
60-4		60		8
45-6-1	6	45		4
45-6-2			6.41	6

Table 4: Mechanical properties of the steel rods

Steel grade	Yield strength N/mm^2	Tensile strength N/mm^2	yield ratio %	Elongation %
SNR400B (φ22)	314	451	70	30

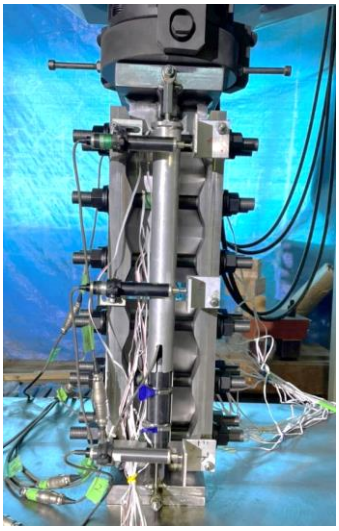

Photo 2: Experimental setup

4.2 Comparison of Experimental Results with Calculated Values

Figure 5 shows the relationship between vertical load (P) and relative displacement (Vd) for each specimen, the various calculated values, and the relationship between value of the vertical load (T_conv.) obtained by converting the load value (T) calculated from the strain of the steel rod using Equation (2) and value (Hd_conv.) obtained by converting the displacement of the expanding up-thrust members (Hd) into vertical displacement based on the geometric relationship. The vertical and horizontal axes represent load value and displacement, respectively. As in the preliminary experiment, we obtained the relationship between the vertical load and the load borne by the steel rods presented in Equation (2) by decomposing the force generated at the tapered section of the tapered member. The coefficient of friction at the interface between the steel members is assumed to be μ = 0.15.

$$P = n \times T \times \frac{2 \times \left(tan\frac{\theta}{2} + \mu\right)}{1 - \mu\, tan\frac{\theta}{2}} \tag{2}$$

P: Vertical load
θ: Angle of the tapered member
T: Force in the axial direction of the steel rods
μ: Coefficient of friction at the interface between steel members
n: Number of steel bars (Tapered member per piece)

In general, the calculated values and the point at which the slope of the curves in the graph changes are in good agreement with the experimental values. We calculated T_conv. as the sum of the load values of the steel rods per tapered member. The relationship with Hd_conv. confirms that the load-bearing behavior is generally as expected. As for the effects of the unloading-reloading process, the unloading stiffness remains low, within the range of the first stiffness. This may be due to the non-uniform distribution of the load borne by the steel rods. This may also be attributed to the lowering of unloading stiffness even before the point of slope change due to the plasticization of the disc springs when they are in complete contact with each other as the secondary stiffness phase is reached.

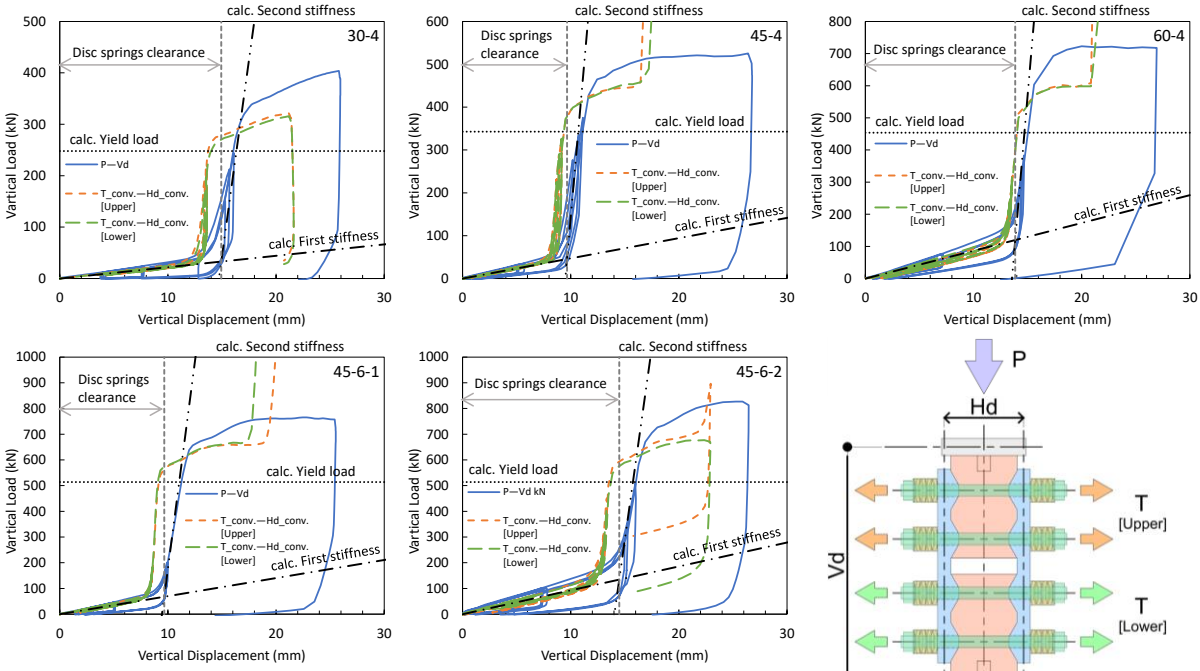

*T is converted into the vertical direction using Equation (2). Hd is converted into the vertical direction based on geometric relationships. The converted values are denoted T_conv. and Hd_conv.

Relationship between load and displacement

Figure 5: Load-displacement relationship

5 ANALYSIS VIA THE FINITE ELEMENT METHOD

To verify the results of the experiments, we undertook an explicit dynamic analysis in the elastic range to compare the experimental and analytical results. We used Ansys LS-DYNA for the analysis.

5.1 The analytical models

Figure 6 shows schematic illustrations of the analytical model. Table 5 presents the parameters used in the analysis. The values of the mechanical properties of the materials used are all nominal values. Figures 6-a and 6-b show the analytical model for the preliminary test specimens and elemental specimens, respectively, having taper angles of 30° and 60°. The tapered members, washers, and foundation are assumed to be rigid bodies, while the up-thrust member and steel rods are assumed to be elastic bodies. Figure 6-c shows the mesh division of the members, each created as a solid model. The coefficient of friction between each member is assumed to be 0.15. Zero friction is assumed between the nut integrated with the steel rod and the washer. Figure 6-d shows how the disc spring is reproduced. The washers and nuts were assembled as shown in the figure, with four spring elements per nut placed in parallel. The stiffness of a single spring element is assumed merely to be the stiffness of the disc spring divided by four. The stiffness of the spring elements is assumed to act only during compression. The height of the washer is defined as the height of the disc springs when they are deformed and in complete contact with each other. Clearance is defined as the total deflection of the disc spring, corresponding to the distance from the washer to the nut joined with the steel rod. The

distance from the up-thrust member to the nut corresponds to the height of the disc springs in the initial state, reproducing how the spring element gradually contracts as the up-thrust member expands and becomes integrated with the steel rod.

In the preliminary test model, with regard to the loading process, the foundation was assumed to be fixed, and load was applied vertically downwards on the two tapered members in the preliminary test model, while in the elemental test model, load was applied vertically downwards on the top tapered member. The tapered member to which load is applied is assumed to be free to translate only in the vertical direction. We assumed translations to be restrained into all other directions and rotations for the sake of stability.

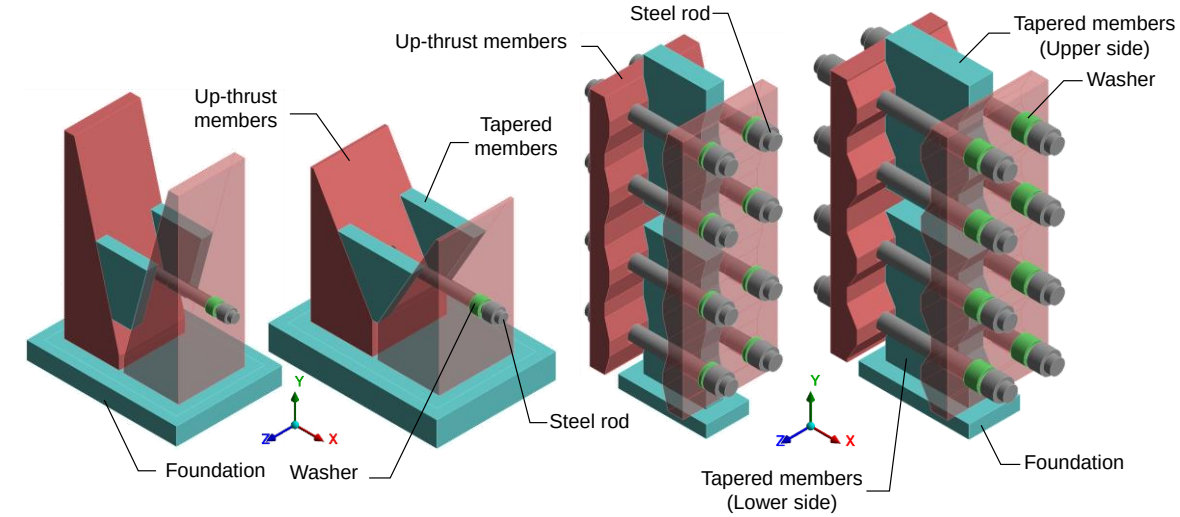

a) Preliminary experiment model (left: 30°; right: 60°)

b) Elemental experiment model (left: 30°; right: 60°)

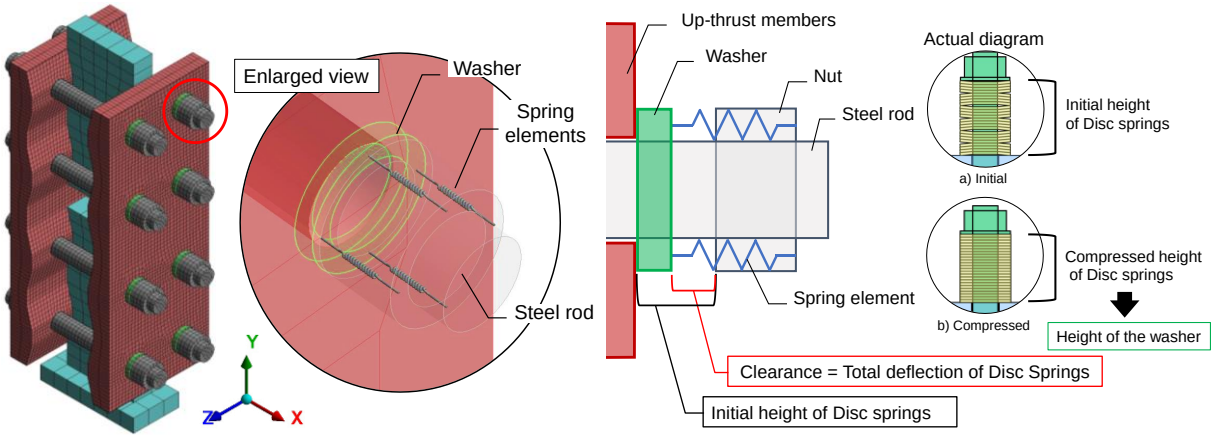

c) Mesh division

d) Modeling of the disc spring

Figure 6: Schematic illustrations of the analytical models

Table 5: Parameters of the analytical models

Case	model	Number of steel rods (Tapered member per piece)	Taper angle °	Disc springs	
				Spring constant kN/mm	Total deflection mm
sim_30-0 sim_60-0	Preliminary	1	30 60	1.04	7.2
sim_30-4 sim_60-4	Elemental	4	30 60	4.81	4 8

5.2 Comparison of Analytical Results with Experimental and Calculated Values

Figure 7 compares the analytical values for each experiment model with the experimental and calculated values, and shows a deformation diagram of the analytical model. The vertical and horizontal axes, respectively, represent load values and displacement. The results show that the values obtained for both models are in general agreement with their respective experimental and calculated values. Additionally, since the positions of the slope change in stiffness obtained for each model are consistent with their calculated values, we concluded that the modeling of the disc springs was appropriate.

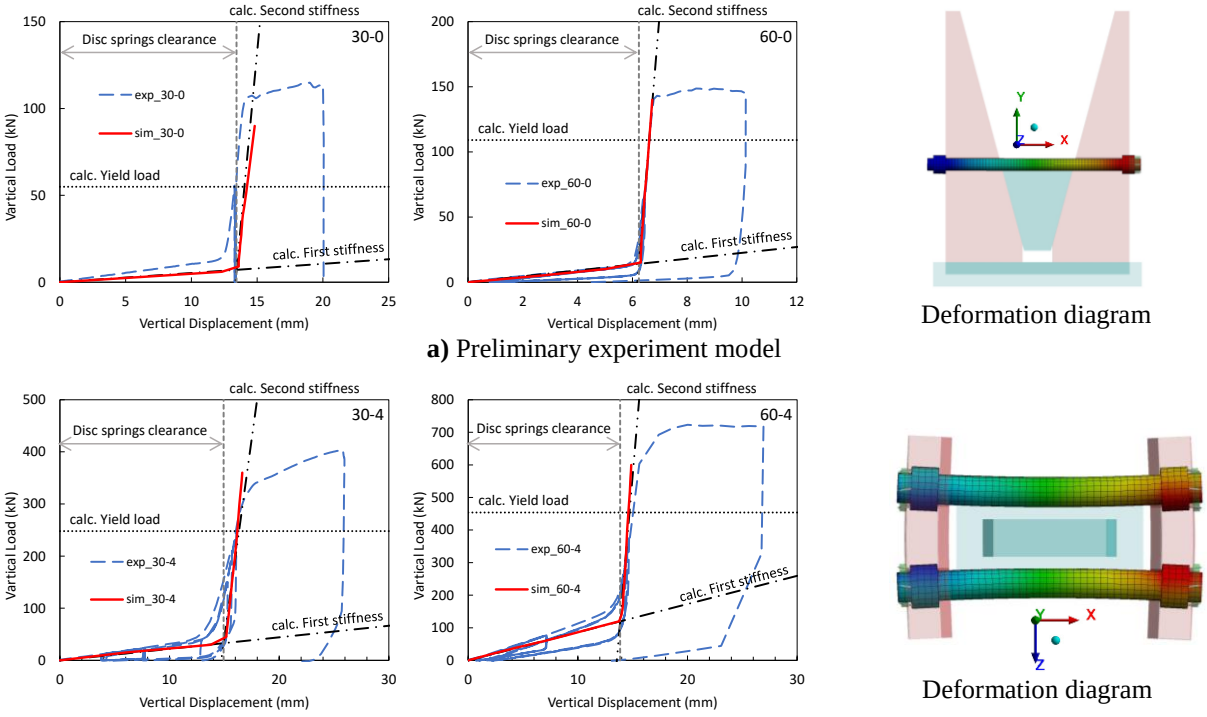

Figure 7: Comparison between analytical results, experimental values, and calculated values, and deformation diagrams

Figure 8 shows the distribution of strain for each position of the steel rods in the elemental experiment and elemental experiment model. The bar graphs show the experimental values, with the horizontal axis indicating the position of the steel rods in the device from top to bottom. Since there is little difference between the analytical values for the steel rods on the left and

right sides, the results for the steel rods in the left column are denoted by broken lines. The experimental values are normalized by dividing the value immediately before the first rod reached the yield strain by its maximum value. The analytical values are divided by the maximum value. While the analytical results for both the 30° and 60° models show a state of nearly uniform load-bearing, the experimental values vary depending on the vertical and horizontal positions of the steel rods. This may be because tension is not controlled when manually tightening the steel rods or because the initial state of the device is relatively unstable, resulting in the load being transferred first to the steel rods initially installed, with relatively smaller disc spring clearance.

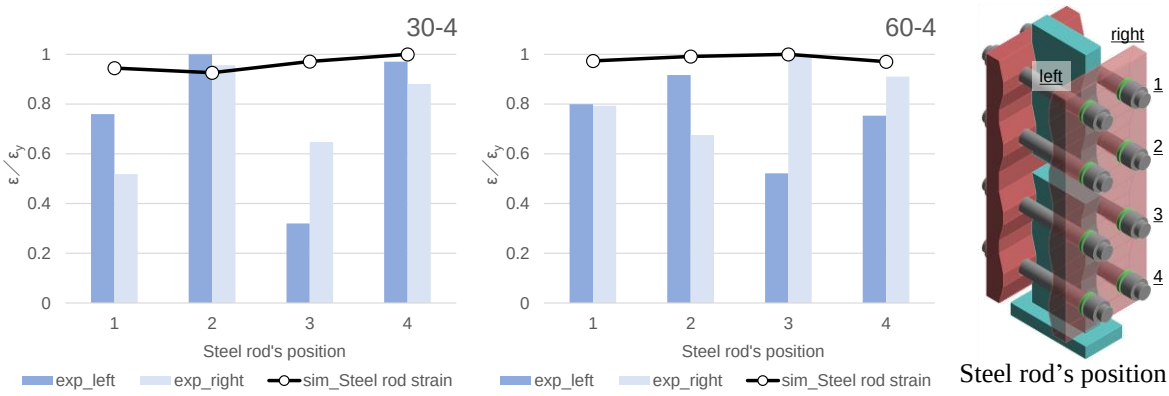

Figure 8: Strain distribution with respect to position of the steel rods

In the preliminary test model, the deformation diagram indicates that no unexpected deformation of the tapered members and the up-thrust members occurs. It also indicates that the load is transferred efficiently through the tapered member. In the elemental experiment model, we observe a bowing-type displacement in the up-thrust member; this deformation is believed to have caused the observed variations in load transfer to the steel rods.

6 SUMMARY

To develop a hardening-type hysteresis element as a control member for suppressing excessive deformation, we undertook preliminary experiments, elemental experiments, and finite element analysis involving the proposed hardening device to confirm its mechanical properties. In addition, we performed a dynamic analysis using a one-degree-of-freedom mass point model to confirm the behavior of the hardening device when the device is applied to a building. Presented below is a summary of our findings.

1) Results of the preliminary experiment confirm that hardening properties exhibiting two levels of stiffness can be realized using a device consisting of tapered members, up-thrust members, steel rods, and disc springs and that the restorative performance can be calculated.
2) As an elemental experiment, we performed a unidirectional loading experiment to verify the specifications of the hardening device when the number of steel rods is increased to strengthen the capacity of the hardening device. The results confirm that capacity can be strengthened as expected.
3) We performed a finite element analysis to reproduce and validate the results of the

preliminary and elemental experiments. The analytical, calculated, and experimental values generally proved to be consistent with each other. We confirmed the difference between the ideal state in the analysis and the actual load bearing distribution of steel rods in the analysis using the elemental experiment model.

REFERENCES

[1] Kana Watanabe, Makoto Yamakawa, and Takeshi Asakawa: Response Control Design of Moment-Resisting Steel Frames Using Displacement-Restraint Brace and Damping Mechanism, Journal of Structural Engineering of the Architectural Institute of Japan, 66B 433–40, 2020